



1 **Advection Impacts the Firn Structure of Greenland's**
2 **Percolation Zone**

3
4
5 Rosemary Leone¹, Joel Harper¹, Toby Meierbachtol¹, and Neil Humphrey²
6
7

8 ¹Department of Geosciences, University of Montana, Missoula MT 59812

9 ²Geology and Geophysics, University of Wyoming, Laramie WY 82071
10
11
12

13 **ABSTRACT.** One dimensional simulations of firn evolution neglect horizontal transport
14 during burial. Using a suite of model runs, we demonstrate the impacts of advection on the
15 development of firn density, temperature, and the stratigraphy of melt features the
16 Greenland ice sheet percolation zone. The simulations isolate processes in synthetic runs,
17 and investigate four specific transects and an ice core site. The advection process tends to
18 increase the pore close-off depth, reduce the heat content, and decrease the frequency of
19 melt features with depth by emplacing firn sourced from higher locations under
20 increasingly warm and melt-affected surface conditions. Horizontal ice flow interacts with
21 topography, climate gradients, and meltwater infiltration to influence the evolution of the
22 firn column structure; the interaction between these variables modulates the impact of
23 advection on firn at locations around Greenland. Pore close-off and firn temperature are
24 mainly impacted in the lowermost 20 km of the percolation zone, which may be relevant to
25 migration of the lower percolation zone. Relatively high in the percolation zone, however,
26 the stratigraphy of melt features can have an advection derived component that should not
27 be conflated with changing climate.
28
29
30
31
32



33 **1. INTRODUCTION**

34 Summer melting of bare ice, epitomized by stream networks and moulins, represents a
35 relatively small portion of the Greenland Ice Sheet (GrIS) periphery since about 90% of the
36 ice sheet's area is perennially snow covered accumulation zone (e.g., Ettema et al., 2009). A
37 large fraction of the snow covered region also experiences melt (Figure 1): between 50-
38 80% melted during summers of the period 1958-2009 (Fettweis et al., 2011), for example.
39 Further, the inland extent and duration of melting have demonstrated increasing trends
40 and have frequently established new records (Mote, 2007; Tedesco, 2007; Tedesco et al.,
41 2013). Melting of the accumulation zone (i.e., the percolation zone) is therefore an
42 increasingly important aspect of the ice sheet, and so too are the glaciological processes
43 governing the snow/firn interactions with surface climate.

44

45 Meltwater from the lower accumulation zone may run off from its point of origin (e.g.,
46 Machguth et al., 2016), while at higher elevations the water may simply infiltrate into cold
47 snow and firn to fill underlying pore space, forming ice when it refreezes (e.g., Braithwaite
48 et al., 1994; Harper et al., 2012) or remaining liquid if it does not (e.g., Forster et al., 2014;
49 Humphrey et al., 2012). While current model fidelity prevents confident constraint on the
50 amount of melt retained in the percolation zone, existing estimates are that 40-50% of the
51 meltwater generated never escapes (van Angelen et al., 2013; Janssens & Huybrechts,
52 2000; Reijmer et al., 2012). However, the evolutionary processes governing many aspects
53 of the framework of the firn column, and thus its ability to accommodate meltwater, are
54 still unclear.

55

56 The percolation zone is a region with relatively high horizontal motion compared to
57 submergence rate (cf. divide regions) (Figure 1). Ice sheet flow displaces the firn column to
58 lower elevation, where it is buried by subsequent winter layers experiencing higher
59 intensity summer melt. Thus, the deep firn column's structural makeup and thermal state
60 results from a climate that varies in both time *and* space. The impact of this effect is
61 undocumented, and likely varies substantially around the ice sheet. Ice motion potentially
62 impacts the structural framework of the firn column, the amount of deep pore space that



63 could absorb meltwater and heat, and the interpretation of melt feature stratigraphy
64 within ice cores collected from these regions.

65

66 Here we investigate the role that horizontal motion plays in driving the structural evolution
67 of the deep firn layer. We utilize previous approaches for modeling firn densification and
68 meltwater infiltration, but extended the analysis to two dimensions to include advection of
69 the domain due to ice flow. Our investigation is focused on synthetic modeling of isolated
70 processes, four differing transects of the GrIS percolation zone, and partitioning the signal
71 of climate change from an advection signal within ice cores from the percolation zone.

72

73 **2. METHODS**

74 **2.1 Model Description**

75 The density and thermal structure of firn within the percolation zone is a function of
76 temperature, accumulation rate, and melt/refreezing processes (Herron and Langway,
77 1980; Reeh et al., 2005). The spatial gradients in these parameters, coupled with the speed
78 at which the ice moves through the gradients, determines the influence of ice flow on deep
79 firn structure. We simulate these processes in a thermo-mechanically coupled framework
80 for firn densification and heat transfer that includes meltwater penetration and refreezing.
81 We employ the most common approach to simulating firn densification, adopt standard
82 physics for heat transfer, incorporate three different approaches to meltwater infiltration,
83 and we do this over a 2D domain accounting for advective displacement. We do not
84 introduce a new suite of physics to the firn modeling community, we explore the impact
85 that advection can have under various conditions on development of a firn column.

86

87 Our modeling incorporates changing surface conditions while ice flow transports the firn
88 column down-glacier by translating time-varying boundary conditions based on surface
89 speed. This approach captures the processes of burial, infiltration, and vertical heat
90 transport, and is advantageous in that it easily accommodates a range of meltwater
91 infiltration schemes (detailed below). It does, however, lack horizontal heat diffusion, but
92 testing against an explicit 2D model for densification and heat transport including
93 horizontal diffusion yielded negligibly different results (Supplementary information; Figure



94 S1). Omission of this process therefore streamlines computational efficiency with little
95 impact on results.

96

97 Firn temperature is modeled by solving the standard one-dimensional time-dependent
98 heat-transfer equation with latent heat from the refreezing of meltwater (Cuffey and
99 Paterson, 2010). We implement the time dependent model for densification from Herron
100 and Langway (1980), based upon it's relatively simplistic formulation with few tuning
101 parameters and favorable comparison with other densification schemes (Lundin et al.,
102 2017). Temperature, density, and vertical velocity were coupled together and solved using
103 the finite element library FeniCS with Galerkin's method. Dirichlet boundaries for state
104 variables temperature, density, and vertical velocity (based on accumulation rate) are
105 imposed at the model surface, and vertical gradients in these variables are set to 0 at the
106 model base.

107

108 Modeling complex and heterogeneous meltwater infiltration in firn remains an outstanding
109 problem of critical importance that solving is beyond the scope of this project. Our
110 approach is to implement three existing infiltration schemes which vary in complexity and
111 reflect a range of approximations. The first model considers only shallow infiltration,
112 assuming that all meltwater refreezes in the top annual layer (Reeh et al., 2005). The
113 second implements a standard tipping bucket method (Kuipers Munneke et al., 2014;
114 Ligtenberg et al., 2018), allowing meltwater infiltration as far as permitted by thresholds
115 for cold content and irreducible water content. Meltwater percolates until reaching a firn
116 layer with a smaller irreducible water content than the available liquid water or the pore
117 close off density is reached; any remaining meltwater runs off instantaneously. The third
118 infiltration model implements a continuum approach (Meyer and Hewitt, 2017), simulating
119 the physics of water flow based on Darcy's Law, and treating both saturated and
120 unsaturated conditions.

121

122 2.3 Model Experiments

123 The influence of horizontal advection on firn structure at depth is dependent on ice flow
124 speed and spatial gradients in climate forcings (temperature, melt, and accumulation). We



125 conducted an initial test of model sensitivity to each of these variables to understand, in
126 isolation, the influence of changes in these processes on firn structure. We then applied the
127 model to four flowline transects across GrIS' percolation zone representing a spectrum of
128 ice sheet and climate conditions.

129

130 2.3.1 Sensitivity Analysis

131 Synthetic sensitivity tests were performed around a base scenario with horizontal velocity
132 of 100 m/yr and an accumulation rate of 0.5 m/yr ice equivalent, approximately matching
133 conditions along the EGIG transect. Horizontal velocities, accumulation rate, and total melt
134 were then varied across ranges of values spanning the conditions that may occur in the
135 GrIS percolation zone (Supplementary information). Additionally, we imposed three
136 different surface temperature gradients in each simulation to determine model sensitivity
137 to a spatially varying surface temperature boundary.

138

139 2.3.2 Greenland Transects

140 Our 2D modeling approach was implemented at four test transects spanning the GrIS
141 (Figure 1): 1) the well-studied EGIG transect in western GrIS, 2) a transect feeding
142 Jakobshavn Isbrae, 3) the K-transect in southwest GrIS, and 4) a transect extending into
143 Helheim Glacier. These four study profiles were selected to capture a wide variety of ice
144 sheet conditions (Table 1). Surface velocities along study transects were defined from
145 satellite velocity data (Joughin et al., 2010), and RACMO2.3p2 (Noël et al., 2018) was used
146 to select 1980-2016 average climate variables (Figure S4). This time period roughly
147 captures the increase in GrIS melt since the late 20th century (Fettweis et al., 2011). In
148 addition to the 2D simulations of the transects, we also completed 1D simulations at 600-
149 1700 locations in each transect, variably spaced between profiles based at annual
150 displacements. The latter were used for baseline comparisons of the effects of including or
151 not including advection of the firn column.

152

153 2.3.3 Core Stratigraphy Example

154 A commonly used metric for quantifying changing climate conditions from firn cores is the
155 annual increment of surface melt, or Melt Feature Percent (MFP) (Graeter et al., 2018;



156 Kameda et al., 1995; Koerner, 1977; Trusel et al., 2018). To investigate the role that
157 advection can play in MFP records, we simulated the specific conditions at Crawford Point
158 located along the EGIG line. This site is relatively high elevation in the percolation zone
159 with far less surface melt than the lower percolation zone. In recent decades the average
160 summer at this site experiences about 15 days of melt (Mote, 2007).

161

162 We modeled the 2D firn evolution on a flow line leading to Crawford Point using datasets
163 for the modern state. Ice surface geometry (Morlighem et al., 2017) and velocity (Joughin et
164 al., 2010) datasets were used for converting from space to time; and, mean melt and
165 snowfall values from RACMO2.3p2 (Noël et al., 2018) were used to determine spatial
166 climate gradients. We assume the spatial gradients in these datasets have not changed over
167 a century time scale. The validity of this assumption is unknown and perhaps tenuous; our
168 intention, however, is a demonstration of the advection process constrained by ice sheet
169 conditions. Furthermore, if there are in fact large time changes in gradients, this only
170 increases complexity to advection signal. Finally, we employ the (Reeh et al., 2005) model
171 for infiltration to be consistent with the assumption of shallow infiltration employed by
172 MFP observational studies.

173

174 **3. RESULTS**

175 **3.1 Sensitivity Tests**

176 Including 2D horizontal advection in simulations of the percolation zone yields greater air
177 content in the firn column and therefore increased depth to pore close off than 1D results
178 (Figure 2; Figure S2). Greater ice flow speed clearly influences advection based results, but
179 the impacts are strongly modulated by the magnitudes and gradients in other variables. For
180 example, the impact of advection is also a function of accumulation, with smaller
181 accumulations causing a 25-35% increase in the depth to pore close off in 2D simulations
182 relative to the 1D model runs. This stems from reduced densification rate under smaller
183 annual increments of overburden, and thus longer preservation of cold and porous firn that
184 becomes deeply buried firn further down-glacier. Adding melt gradients to the scenarios
185 exacerbates the effect, with wet surface conditions overprinting dryer conditions at depth.

186



187 Adding advection to simulations also decreases the firn temperature; the temperature
188 profile and temperature at pore close off reflect advected firn from higher, colder
189 conditions. Heat content is strongly influenced by choice of melt scheme: for example,
190 under very high accumulation and melt, the tipping bucket method yields deep penetration
191 of water and warmer firn temperature at depth (cf. the 1D case). Steeper topography yields
192 larger along-flow gradients between melt, temperature, and accumulation, causing greater
193 disparities between 2D-advection and 1D-profile simulations. The ice flow speed has
194 potential to strongly impact simulations with 2D-advection, but importantly, the impact of
195 speed is strongly modulated by the values and gradients in other variables. In simulations
196 of high horizontal gradients in climate (i.e., steep topography), and limited melt
197 penetration (i.e., infiltration following Reeh et al. (2005)), model results including ice flow
198 differ from 1D by up to four-fold at highest speeds.

199

200 3.2 Transects

201 The most significant differences between the 1D and 2D model simulations are along the
202 lowermost 10-15 km of our four sample transects. Here, surface speed and slope (a proxy
203 for climate gradients) both increase substantially relative to the upper percolation zone,
204 and the surface experiences heavy melt. By including ice flow in these firn simulations, the
205 density differs by $>50 \text{ kg m}^{-3}$ for the EGIG, Jakobshavn, and Helheim transects (Figure 3;
206 Figure S4; Figure S5), resulting in increases to pore close off depth of up to 8 m, 13 m, and
207 19 m, respectively. The commensurate impacts on total air content in the firn column can
208 also be large: for example, along the EGIG transect it changes by $\sim 50\%$ in the lower 10 km,
209 and by 5%-15% along the next 10-20 km.

210

211 The different melt infiltration schemes yield variable impacts. The largest impact is with
212 the Reeh et al. (2005) scheme, under which the inclusion of advection in simulations
213 increases the firn column air content by up to several meters from a 1D simulation (Figure
214 4). Local changes in surface slope along the transects both enhance and diminish the
215 impacts of advection on the underlying firn structure, complicating the 2D firn geometry of
216 the percolation zone. The changes to density structure throughout the K-transect are



217 comparatively small because the topography and speeds are so much lower than most
218 places on the ice sheet (Table 1), all but eliminating the impact of ice flow (Figure 3d).

219

220 The process of advection generates colder firn temperature profiles. Along the EGIG
221 transect advection decreases firn temperatures at the depth to pore close off by 1.0°-1.5° C
222 in the lower 15 km, and by 0.8°-1.0° C in the next 15 km. With the high speeds, steep
223 topography, and heavy melt of the lowermost reaches of Jakobshavn and Helheim
224 transects, firn temperatures were altered by as much as 3° C by including advection.

225

226 3.3. Core Stratigraphy Example

227 Our modeling indicates that at Crawford Point, the depth (time) change in MFP that is
228 attributable to advection alone is inconsequential in firn generated in recent decades (i.e.,
229 <60m depth). The shallower firn was deposited along the first ~5km above Crawford Point,
230 a region with very low slope and essentially no horizontal climate gradient caused by
231 elevation. Below this depth, however, there is an abrupt inflection to continuously
232 decreasing MFP to the bottom of the core (Figure 5). At depths >60 m, the change in MFP
233 due to advection amounts to about 0.04% per year. As discussed below, this is a non-trivial
234 magnitude when scaled against the annual change arising from warming climate and
235 increased melt.

236

237 4. DISCUSSION

238 4.1. Uncertainty due to Infiltration

239 The choice of meltwater infiltration scheme has a large effect on the simulated impacts of
240 firn advection in the percolation zone and is a key uncertainty in the fidelity of model
241 results. In reality, water moves vertically as a wetting front propagating downward from
242 the surface (Colbeck, 1975), but also by complex and unpredictable inhomogeneous
243 infiltration processes (Marsh and Woo, 1984; Pfeffer and Humphrey, 1996), and it can be
244 routed horizontally along impermeable ice layers (e.g., Machguth et al., 2016). With so little
245 known about deep infiltration, none of our schemes are likely to be entirely accurate: the
246 (Reeh et al., 2005) scheme only allows melt penetration within the annual snow increment
247 which is known to be incorrect, especially low in the percolation zone where melt rates are



248 high (e.g., Humphrey et al., 2012); the continuum model (Meyer and Hewitt, 2017) uses the
249 most complex physics, but has large uncertainties for coefficients of permeability and grain
250 sizes; and, the tipping bucket model (Kuipers Munneke et al., 2014; Ligtenberg et al., 2018)
251 disregards the complex physics governing flow of water through its own solid matrix,
252 simplifying the problem to just density and cold content and assuming the flow of
253 meltwater is instantaneous.

254

255 With firn advection tending to move open pore space underneath an increasingly melting
256 surface, the depth/quantity of infiltration is key: the deeper melt penetrates, the more the
257 pore space is 'overprinted' by surface melt and the advected deep pore space is not
258 preserved. Alternatively, infiltration that is limited to shallow depths enhances the
259 disparity between deep firn and that nearer to the surface. Our suite of model runs show
260 that, in the lower percolation zone, the choice of infiltration scheme has nearly equivalent
261 impact on the total air content as the incorporation of ice flow.

262

263 4.2. Melt Feature Stratigraphy

264 A 152 m long ice core collected at Crawford Point in 2007 (Higgins, 2012; Porter and
265 Mosley-Thompson, 2014) offers the opportunity to compare measured data against our
266 modeled depth change in MFP stemming from advection. The core age extends back to the
267 year 1765 based on seasonal isotope variations, and the modeled flow field shows the
268 bottom of the core originated ~260 years prior and about ~22 km up the flow line (Figure
269 5a). Thus, the flow model age estimate at the core-bottom is within 7% of the age
270 determined by isotope methods. Higgins (2012) measured an overall trend of increasing
271 MFP from 1765-2007 of 0.08% per year. However, melt events prior to 1900 were minor
272 and infrequent; the more recent trend from 1900-2007 therefore increases to 0.11% per
273 year.

274

275 The advection signal we calculate is also highly dependent on the defined time period, but
276 for a much another reason: different time periods sample different spatial gradients in
277 climate as firn moves through the percolation zone. The MFP signal in firn from recent
278 decades is not influenced by advection because this firn has formed along a locally flat spot



279 in the topography extending about 5 km up flow from Crawford Point (Figure 5a).
280 However, over the ~100 years during which significant melt increases are observed in the
281 core, our modeling suggests that approximately one third of the MPF change is attributable
282 to the advection process (Figure 5b). Thus, the stratigraphy of melt features along an ice
283 core from the percolation zone can have a spatial component that must be evaluated to
284 properly interpret temporal change.

285

286 That profiles of firn density and temperature are barely impacted by advection at Crawford
287 Point, yet the MFP record is strongly influenced by advection, may seem counterintuitive.
288 However, these are different entities: the former firn properties evolve over a time-space
289 continuum, whereas the MFP record represents a time-trend in the occurrence of discrete
290 events. Furthermore, the magnitude of trends sets the importance of advection in a MFP
291 record. In the Crawford case, the multi-decadal trend in MFP due to changing melt is a
292 fraction of a percent per year, an important indicator of changing climate, but not large
293 enough to completely mask advection. Where the advection signal is strong it may be likely
294 that it is equivalent to the climate trend.

295

296 Certainly some locations in the percolation zone may yield ice cores with MFP trends that
297 are not significantly impacted by ice flow. But considering the potential for ice flow to
298 obscure climate trends, a simple procedure for quantifying this effect has utility. If the
299 present ice sheet state (speed, accumulation, and melt rates) is assumed to be constant in
300 time, an apparent climate signal at any core site can be quantified from spatially extensive
301 datasets of the above variables. At a core depth corresponding to a time before present (t),
302 the firn package originated at a location (x) upglacier from the core location, where x is the
303 integral of the spatially varying velocity (v) along the flowline over t years:

$$x(t) = - \int_0^t v(x) dt. \quad (1)$$

304 The MFP at time (t) can be determined from the accumulation and melt conditions at this
305 upglacier location:

$$MFP(x) = \frac{m(x)}{b(x)}. \quad (2)$$



306 Equations 1 and 2 can thus be combined to generate a time series of MFP that is a record of
307 spatially varying climate advected by ice flow; the component that should not be
308 incorrectly interpreted as time-changing climate.

309

310 **5. CONCLUSIONS**

311 Elevated horizontal ice flow in the percolation zone compared to ice divides results in a firn
312 column that is not always well represented by 1D models for time-evolving density and
313 temperature. The impacts of advection are highly variable around the ice sheet, but
314 accounting for advection in simulations can change the firn's air content by 10s of percent
315 and the temperature can differ by several degrees. Lower accumulation, higher velocity,
316 higher melt, and steeper topography (which drives climate gradients) all increase the
317 mismatch between surface and deep conditions (and the failure of a 1D simulation). The
318 advection process thus has greatest influence on firn evolution in the lower accumulation
319 zone (e.g., 10-15 km); a nexus of conditions that are likely migrating upward as climate
320 warms but are also subject to the greatest uncertainty regarding melt infiltration
321 processes.

322

323 The 2D evolution of firn in the percolation zone is influenced by topography: horizontally
324 invariant firn is generated in flat regions, whereas local hills/swales enhance the 2D
325 influences from advection. The deeper meltwater penetrates, the more pore space is filled
326 by surface melt and the advected deep pore space and cold content is not preserved. The
327 stratigraphy of melt features along an ice core from the percolation zone can have a strong
328 spatially derived component. Melt feature stratigraphy can be impacted by advection high
329 in the percolation zone, where firn density and temperature are relatively unaffected by ice
330 flow. This effect must be evaluated to properly interpret temporal changes in ice cores
331 related to climate, especially over decadal and longer time scales.

332

333 **ACKNOWLEDGEMENTS**

334 Funded by NSF grants 1717241 (Harper, Meierbachtol) and 1717939 (Humphrey), and a
335 Montana NASA Space Grant Fellowship to Rosie Leone. This paper has no data to declare.

336



337 **REFERENCES CITED**

- 338 Van Angelen, J. H., Lenaerts, J. T. M., Van Den Broeke, M. R., Fettweis, X. and Van Meijgaard,
339 E.: Rapid loss of firn pore space accelerates 21st century Greenland mass loss,
340 Geophys. Res. Lett., 40(10), 2109–2113, doi:10.1002/grl.50490, 2013.
- 341 Braithwaite, R. J., Laternser, M. and Pfeffer, W. T.: Variations of near-surface firn density in
342 the lower accumulation area of the Greenland ice sheet, Pakitsoq, West Greenland, J.
343 Glaciol., 40(136), 477–485, doi:10.1017/S002214300001234X, 1994.
- 344 Colbeck, S. C.: A theory for water flow through a layered snowpack, Water Resour. Res.,
345 11(2), 261–266, doi:10.1029/WR011i002p00261, 1975.
- 346 Cuffey, K. M. and Paterson, W. S. B.: The physics of glaciers, 4th Edition., 2010.
- 347 Ettema, J., Van Den Broeke, M. R., Van Meijgaard, E., Van De Berg, W. J., Bamber, J. L., Box, J.
348 E. and Bales, R. C.: Higher surface mass balance of the Greenland ice sheet revealed by
349 high-resolution climate modeling, Geophys. Res. Lett., 36(12), 4–8,
350 doi:10.1029/2009GL038110, 2009.
- 351 Fettweis, X., Tedesco, M., Van Den Broeke, M. and Ettema, J.: Melting trends over the
352 Greenland ice sheet (1958–2009) from spaceborne microwave data and regional
353 climate models, Cryosphere, 5(2), 359–375, doi:10.5194/tc-5-359-2011, 2011.
- 354 Forster, R. R., Box, J. E., Van Den Broeke, M. R., Miège, C., Burgess, E. W., Van Angelen, J. H.,
355 Lenaerts, J. T. M., Koenig, L. S., Paden, J., Lewis, C., Gogineni, S. P., Leuschen, C. and
356 McConnell, J. R.: Extensive liquid meltwater storage in firn within the Greenland ice
357 sheet, Nat. Geosci., 7(2), 95–98, doi:10.1038/ngeo2043, 2014.
- 358 Graeter, K. A., Osterberg, E. C., Ferris, D. G., Hawley, R. L., Marshall, H. P., Lewis, G., Meehan,
359 T., McCarthy, F., Overly, T. and Birkel, S. D.: Ice Core Records of West Greenland Melt
360 and Climate Forcing, Geophys. Res. Lett., 45(7), 3164–3172,
361 doi:10.1002/2017GL076641, 2018.
- 362 Harper, J., Humphrey, N., Pfeffer, W. T., Brown, J. and Fettweis, X.: Greenland ice-sheet
363 contribution to sea-level rise buffered by meltwater storage in firn, Nature,
364 491(7423), 240–243, doi:10.1038/nature11566, 2012.
- 365 Herron, M. M. and Langway, C. C.: Firn densification: an empirical model., J. Glaciol., 25(93),
366 373–385, doi:10.1017/S0022143000015239, 1980.
- 367 Higgins, L.: Construction and Analysis of an Ice Core-Derived Melt History from West



- 368 Central Greenland (1765-2006), The Ohio State University., 2012.
- 369 Humphrey, N. F., Harper, J. T. and Pfeffer, W. T.: Thermal tracking of meltwater retention in
370 Greenland's accumulation area, *J. Geophys. Res.*, 117(F1), F01010,
371 doi:10.1029/2011JF002083, 2012.
- 372 Janssens, I. and Huybrechts, P.: The treatment of meltwater retention in mass-balance
373 parameterizations of the Greenland ice sheet, *Ann. Glaciol.*, 31(1), 133–140,
374 doi:10.3189/172756400781819941, 2000.
- 375 Joughin, I., Smith, B. E., Howat, I. M., Scambos, T. and Moon, T.: Greenland flow variability
376 from ice-sheet-wide velocity mapping, *J. Glaciol.*, 56(197), 415–430,
377 doi:10.3189/002214310792447734, 2010.
- 378 Kameda, T., Arita, N., Ulii, F. and Atanabe, W.: Melt features in ice cores from Site, *Ann.*
379 *Glaciol.*, 21(June 1989), 51–58, 1995.
- 380 Koerner, R. M.: Devon Island Ice Cap: Core Stratigraphy and Paleoclimate, *Science* (80-.),
381 196(4285), 15–18, doi:10.1126/science.196.4285.15, 1977.
- 382 Kuipers Munneke, P., Ligtenberg, S. R. M., Van Den Broeke, M. R., Van Angelen, J. H. and
383 Forster, R. R.: Explaining the presence of perennial liquid water bodies in the firn of
384 the Greenland Ice Sheet, *Geophys. Res. Lett.*, 41(2), 476–483,
385 doi:10.1002/2013GL058389, 2014.
- 386 Ligtenberg, S. R. M., Munneke, P. K., Noël, B. P. Y. and Van Den Broeke, M. R.: Brief
387 communication: Improved simulation of the present-day Greenland firn layer (1960-
388 2016), *Cryosphere*, 12(5), 1643–1649, doi:10.5194/tc-12-1643-2018, 2018.
- 389 Lundin, J. M. D., Stevens, C. M., Arthern, R., Buizert, C., Orsi, A., Ligtenberg, S. R. M.,
390 Simonsen, S. B., Cummings, E., Essery, R., Leahy, W., Harris, P., Helsen, M. M. and
391 Waddington, E. D.: Firn Model Intercomparison Experiment (FirnMICE), *J. Glaciol.*,
392 63(239), 401–422, doi:10.1017/jog.2016.114, 2017.
- 393 Machguth, H., Macferrin, M., Van As, D., Box, J. E., Charalampidis, C., Colgan, W., Fausto, R. S.,
394 Meijer, H. A. J., Mosley-Thompson, E. and Van De Wal, R. S. W.: Greenland meltwater
395 storage in firn limited by near-surface ice formation, *Nat. Clim. Chang.*, 6(4), 390–393,
396 doi:10.1038/nclimate2899, 2016.
- 397 Marsh, P. and Woo, M. -K: Wetting front advance and freezing of meltwater within a snow
398 cover: 1. Observations in the Canadian Arctic, *Water Resour. Res.*, 20(12), 1853–1864,



- 399 doi:10.1029/WR020i012p01853, 1984.
- 400 Meyer, C. R. and Hewitt, I. J.: A continuum model for meltwater flow through compacting
401 snow, *Cryosphere*, 11(6), 2799–2813, doi:10.5194/tc-11-2799-2017, 2017.
- 402 Morlighem, M., Williams, C. N., Rignot, E., An, L., Arndt, J. E., Bamber, J. L., Catania, G.,
403 Chauché, N., Dowdeswell, J. A., Dorschel, B., Fenty, I., Hogan, K., Howat, I., Hubbard, A.,
404 Jakobsson, M., Jordan, T. M., Kjeldsen, K. K., Millan, R., Mayer, L., Mouginit, J., Noël, B. P.
405 Y., O’Cofaigh, C., Palmer, S., Rysgaard, S., Seroussi, H., Siegert, M. J., Slabon, P., Straneo,
406 F., van den Broeke, M. R., Weinrebe, W., Wood, M. and Zinglensen, K. B.: BedMachine
407 v3: Complete Bed Topography and Ocean Bathymetry Mapping of Greenland From
408 Multibeam Echo Sounding Combined With Mass Conservation, *Geophys. Res. Lett.*,
409 44(21), 11,051–11,061, doi:10.1002/2017GL074954, 2017.
- 410 Mote, T. L.: Greenland surface melt trends 1973–2007: Evidence of a large increase in 2007,
411 *Geophys. Res. Lett.*, 34(22), 1–5, doi:10.1029/2007GL031976, 2007.
- 412 Noël, B., Van De Berg, W. J., Van Wessem, J. M., Van Meijgaard, E., Van As, D., Lenaerts, J. T.
413 M., Lhermitte, S., Munneke, P. K., Smeets, C. J. P. P., Van Uft, L. H., Van De Wal, R. S. W.
414 and Van Den Broeke, M. R.: Modelling the climate and surface mass balance of polar
415 ice sheets using RACMO2 - Part 1: Greenland (1958–2016), *Cryosphere*, 12(3), 811–
416 831, doi:10.5194/tc-12-811-2018, 2018.
- 417 Pfeffer, W. T. and Humphrey, N. F.: Determination of timing and location of water
418 movement and ice-layer formation by temperature measurements in sub-freezing
419 snow, *J. Glaciol.*, 42(141), 292–304, doi:10.1017/S0022143000004159, 1996.
- 420 Porter, S. E. and Mosley-Thompson, E.: Exploring seasonal accumulation bias in a west
421 central Greenland ice core with observed and reanalyzed data, *J. Glaciol.*, 60(224),
422 1093–1100, doi:10.3189/2014JogG13J233, 2014.
- 423 Reeh, N., Fisher, D. A., Koerner, R. M. and Clausen, H. B.: An empirical firn-densification
424 model comprising ice lenses, in *Annals of Glaciology*, vol. 42, pp. 101–106., 2005.
- 425 Reijmer, C. H., Van Den Broeke, M. R., Fettweis, X., Ettema, J. and Stap, L. B.: Refreezing on
426 the Greenland ice sheet: A comparison of parameterizations, *Cryosphere*, 6(4), 743–
427 762, doi:10.5194/tc-6-743-2012, 2012.
- 428 Tedesco, M.: Snowmelt detection over the Greenland ice sheet from SSM/I brightness
429 temperature daily variations, *Geophys. Res. Lett.*, 34(2), 1–6,



430 doi:10.1029/2006GL028466, 2007.

431 Tedesco, M., Fettweis, X., Mote, T., Wahr, J., Alexander, P., Box, J. E. and Wouters, B.:
432 Evidence and analysis of 2012 Greenland records from spaceborne observations, a
433 regional climate model and reanalysis data, *Cryosph.*, 7(2), 615–630, doi:10.5194/tc-
434 7-615-2013, 2013.

435 Trusel, L. D., Das, S. B., Osman, M. B., Evans, M. J., Smith, B. E., Fettweis, X., McConnell, J. R.,
436 Noël, B. P. Y. and van den Broeke, M. R.: Nonlinear rise in Greenland runoff in response
437 to post-industrial Arctic warming, *Nature*, 564(7734), 104–108, doi:10.1038/s41586-
438 018-0752-4, 2018.

439

440

441

442

443

444

445

446

447

448

449

450

451

452

453

454

455

456

457

458

459

460

461

462

463

464

465

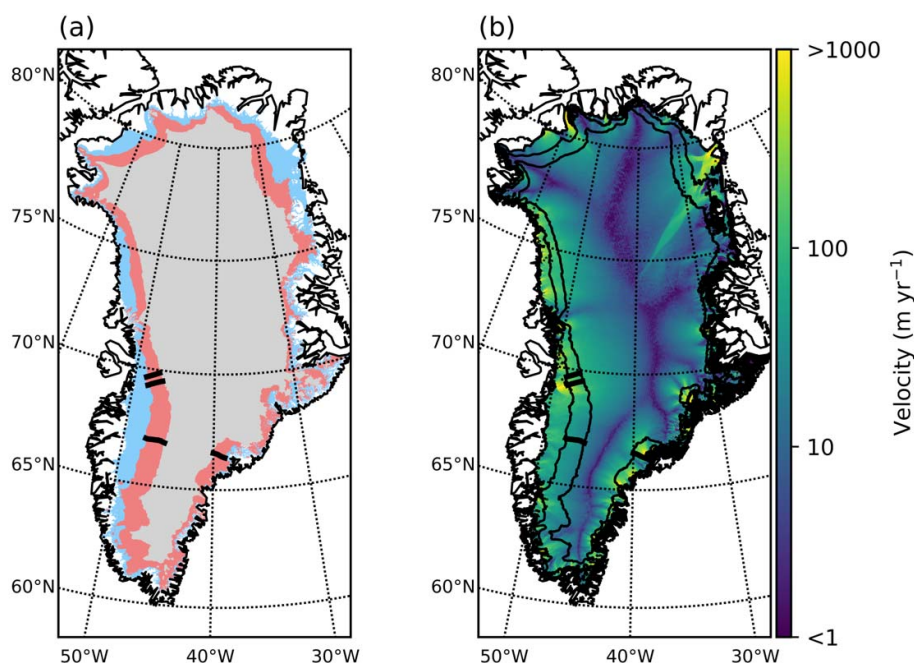
466

467

468



469



470

471

472

473

474

475

476

477

478

479

480

481

482

483

484

485

486

487

488

489

490

491

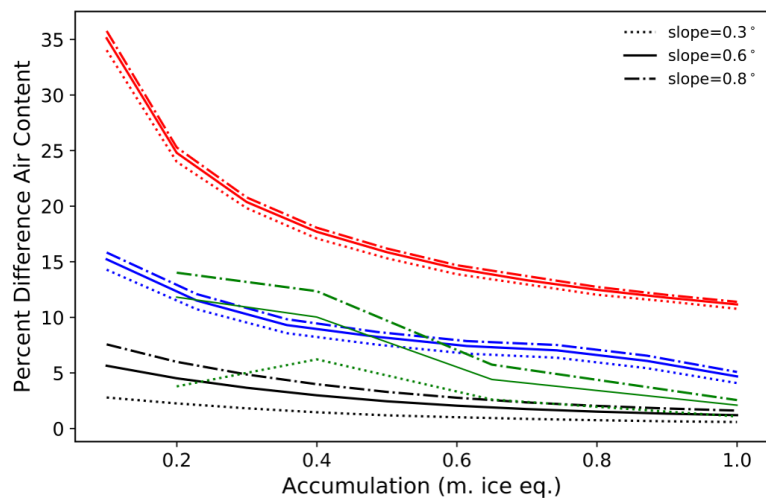
492

493

Figure 1. Maps of Greenland. (a) Facies arbitrarily delineated based on modeled 1980-2016 average surface melt (Noël et al., 2018): ablation zone (red) with melt exceeding accumulation; percolation zone (yellow), the upper limit of which defined by melt conditions at Crawford Point where infiltration has not warmed firn (Humphrey et al., 2012); dry zone (blue). (b) velocity field from Joughin et al. (2010) with top and bottom of percolation zone shown in (a) delineated by black contour lines. Thick black lines through percolation zone show study transects, where E is EGIG, J is Jakobshavn, K is K-transect, H is Helheim (see Table 1).



494



495

496

497

498

499

500

501

502

503

504

505

506

507

508

509

510

511

512

513

514

515

516

517

518

519

520

521

522

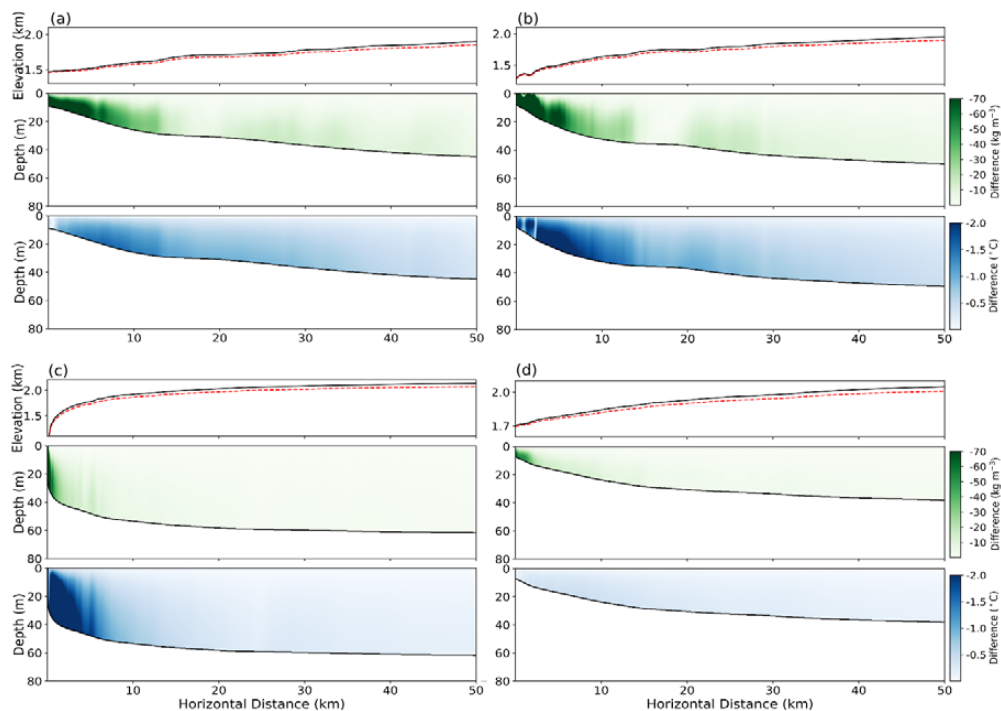
523

524

Figure 2. Example sensitivity test. Modeled differences between 1D and 2D for accumulation using dry model (black), Reeh model (red), tipping bucket model (blue), and continuum model (green). Base speed is 100 m a^{-1} , approximately the lowest value of the EGIG transection shown in Figure 1. Three slopes are used to represent different conditions around the ice sheet.



525



526

527

528

529

530

531

532

533

534

535

536

537

538

539

540

541

542

543

544

545

546

547

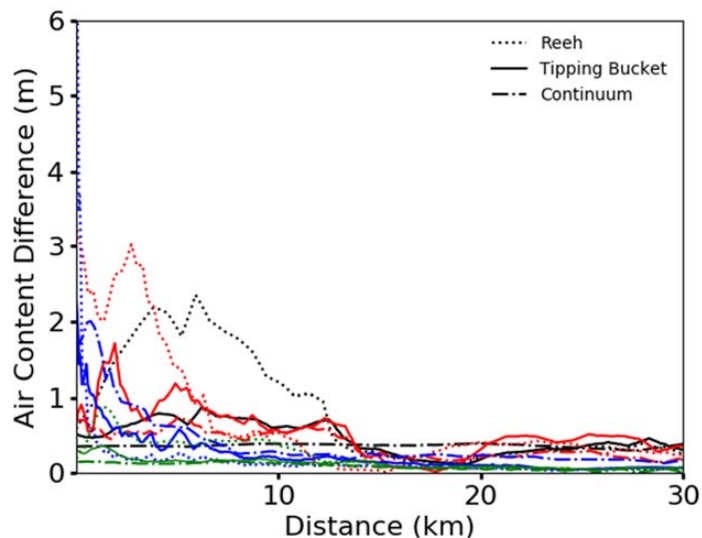
548

549

Figure 3. Calculated difference between 2D and 1D simulated firn properties in the percolation zone through the four study transects with tipping bucket meltwater infiltration scheme: a) EGIG line; b) Jakobshavn; c) Helheim; and, d) K-transect. Top panel in each transect shows surface topography (black) and pore close-off depth (red dashed). Middle panel shows density differences (2D - 1D), and bottom panel shows temperature differences.



550

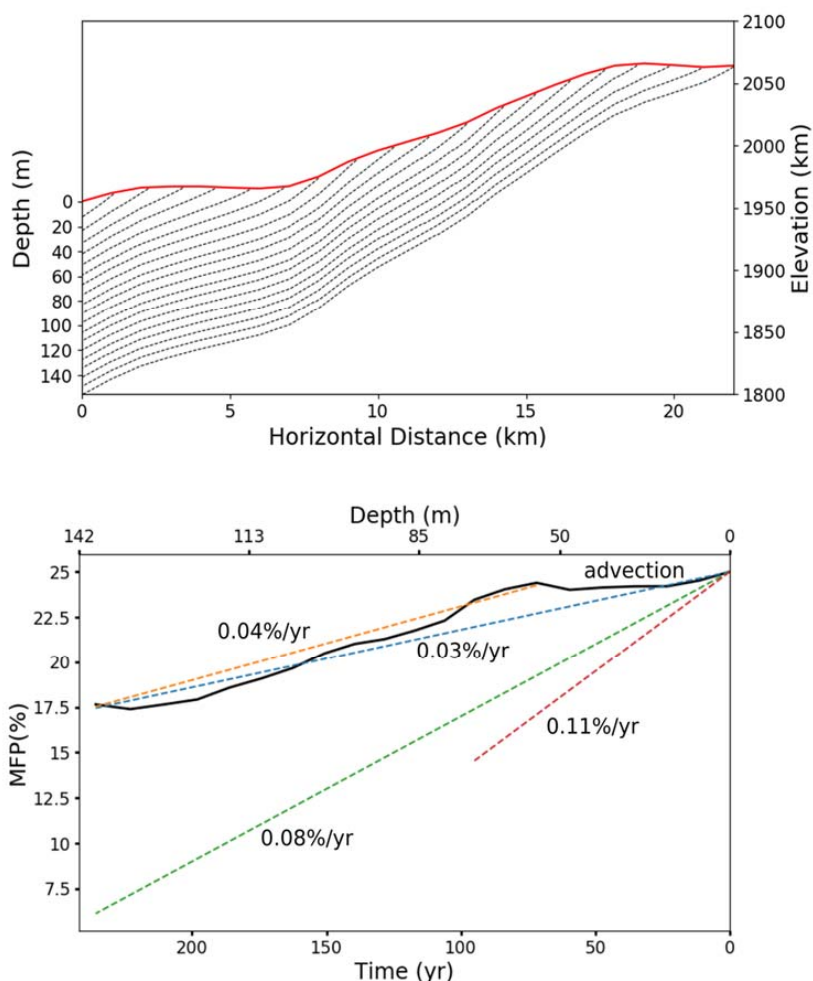


551
552
553
554
555
556
557
558
559
560
561
562
563
564
565
566
567
568
569
570
571
572
573
574
575
576
577

Figure 4. Simulated difference between in integrated firn air content 2D and 1D modeling schemes. Differences are presented for each meltwater infiltration scheme: Reeh et al. (2005) (dotted), tipping bucket (solid), and continuum (dash-dotted). EGIG study transect is shown in black, Jakobshavn in red, Helheim in blue, and K-transect in green.



578



579 **Figure 5.** Surface topography and modeled flow lines extending inland from Crawford
580 Point (a). Horizontal distance scale is kilometers from Crawford Point. Bottom panel (b)
581 shows the modeled change in MFP over time (bottom axis) and with depth (top axis)
582 resulting from ice flow alone. Depth scale in (b) corresponds to firn depth in (a). Time
583 trends in calculated MFP are shown for the full time/depth period (blue) and for the firn
584 profile below 60 m (orange). Time trends in MFP measured in a Crawford Point ice core
585 and reported by Higgins (2012) entire period (green) and the 1900-2007 period (red) are
586 shown for reference.
587

588
589
590
591



592

593

Table 1. Approximate conditions along the four transects used in the study.

Transect	EGIG	Jakobshavn	K-transect	Helheim
Elevation Range (m)	1470-1950	1290-2020	1700-2082	1232-2160
Speed (m yr ⁻¹)	93-150	85-400	27-71	35-1900
Snowfall (m ice equiv)	0.46	0.55	0.4	0.7-1.3
Temperature (°C)	-14° to -18°	-13° to -18°	-9° to -18°	-15° to -17°
Melt (m ice equiv)	0.11-0.43	0.1-0.53	0.15-0.4	0.1-1.3

594